Geophys. J. Int. (1991) **107**, 83–94

On the distribution of anomalous mass within the Earth: forward models of the gravitational potential spectrum using ensembles of discrete mass elements

Michael J. Jackson,* Henry N. Pollack and Stephen T. Sutton†
Department of Geological Sciences, The University of Michigan, Ann Arbor, MI 48109, *USA*

Accepted 1991 April 29; Received 1991 April 29; in original form 1990 August 28

SUMMARY

We investigate forward models of the gravitational potential spectrum generated by ensembles of discrete sources of anomalous mass, having radial distributions with different statistical properties. Models with a random distribution of point source locations throughout the volume of the mantle produce spectra similar to that of the Earth only when the (absolute) source magnitudes increase strongly with depth, at least as $d^{1.5}$. The effects of the geographic (latitude–longitude) distribution of source locations are generally unimportant in determining the general degree dependence of the potential spectrum. The dimensions of the sources are also of secondary importance, at least up to an angular diameter of about 40°, i.e., continent-sized. Sources of this size confined to the upper mantle do not appear capable of producing the degree dependence of the observed geopotential spectrum; the low harmonics (2–4) in particular appear to require lower mantle sources of considerable strength. Further, at least some of these deep sources must be largely monopolar in nature, (i.e., uncompensated) due to the stronger depth attenuation of dipole (compensated) sources. Because topography on the core–mantle boundary must be either isostatically or dynamically compensated, it may contribute little strength to the observed potential spectrum.

Key words: geodynamics, geoid, gravity, mantle, potential.

1 INTRODUCTION

The Earth's non-hydrostatic gravitational potential reflects the presence of lateral density contrasts within its interior. These contrasts may arise in the mantle as a consequence of lateral temperature gradients, compositional heterogeneities, and dynamically maintained topography on internal density interfaces. In a number of previous studies (e.g., Lambeck 1976; Lowrey 1978; Cook 1980; Bowin 1983, 1986; Bowin, Scheer & Smith 1986), it has been suggested that the spherical harmonic spectrum of the non-hydrostatic gravitational potential contains important general information on the distribution of anomalous mass within the mantle. However, the conclusions drawn in these studies regarding the distribution of internal mass anomalies have been contradictory.

Lambeck (1976) suggested that the degree-dependence of the spectrum over the interval $2 \leq n \leq 18$ could be accounted for by a random distribution of density anomalies in the upper 1000 km of the mantle. Lowrey (1978), on the other hand, concluded that anomalous masses increasing (in number and/or magnitude) with depth provide a better match for the observed spectrum. In the model of Cook (1980), the dominant sources of the harmonics up to degree 9 are located in the lower mantle, whereas higher harmonics arise from upper mantle sources. Bowin (1983, 1986) concluded that the degree 2 and 3 harmonics are generated principally by sources at the core–mantle boundary.

Because of the correlation of the gravitational potential and topography at high degrees, it is likely that these harmonics have shallow sources (Phillips & Lambeck 1980). Similarly, Hager (1984) has shown that a model geoid produced by deep slab penetration and dynamic topography on the core–mantle boundary (CMB) exhibits a statistically significant correlation with the actual geoid over the harmonic range $4 \leq n \leq 9$. This leads to the non-unique but physically appealing interpretation that the spectral strength in that interval derives dominantly from dynamic density anomalies associated with subduction.

* Currently at: University of Minnesota, Minneapolis, MN, USA.
† Currently at: Exxon Company International, Houston, TX, USA.

Sutton, Pollack & Jackson (this issue, paper I) present analytical tools for forward modelling of the geoid and its spectrum using discrete internal sources. In this paper we utilize this methodology (see paper I for symbol definitions) to explore forward models of the spectrum arising from various model distributions of anomalous mass, with special emphasis on the radial distribution.

An important aspect of our approach is that we seek to establish important but relatively general properties of the distribution of internal mass anomalies. We are not concerned with reproducing the actual geographic configuration of the geoid; we will focus entirely on obtaining model distributions of amplitudes and wavelengths comparable to those of the actual geoid. We will show that these spectral characteristics are largely insensitive to the geographic distribution of anomalous sources, as well as to their physical dimensions, at least up to about degree 10 of the potential spectrum. Thus we will reach the conclusion that the principal control on the degree-dependence of the spectrum is the radial distribution of anomalous mass.

In essence, we attempt to reduce the intrinsic non-unqueness of potential field source modelling by eliminating *a priori* one degree of freedom in the source models, namely the geographic (latitude–longitude) distribution. Although we employ 3-D source distributions, we are ultimately interested in obtaining 1-D view of the distribution of mass heterogeneities in the mantle: the horizontally integrated radial distribution. By examining the statistical properties of the 'successful' subset of randomly generated source ensembles, i.e., those that yield spectra similar to that observed for the Earth, we may be able to draw general conclusions about the statistical distribution of anomalous mass with depth in the mantle. In terms of geodynamic processes, such as mantle convection, these general properties may be considered to characterize the general convective condition, whereas the actual geoid is representative of one particular (the present-day) realization of that condition.

We note at the outset that the use of discrete sources of anomalous mass as modelling elements involves in inherent assumption about the nature of the heterogeneity within the Earth, just as smoothly varying anomalous density functions do. Discrete source modelling elements, by virtue of the density discontinuities on their boundaries, can be considered relatively 'white' sources, i.e., they are capable of generating geoidal variations at all wavelengths or all harmonic degrees, depending on their depth. As shown in paper I, depth acts as a low-pass filter, through which 'white' sources produce 'red' potential spectra at the surface. Smoother density models, such as low-degree spherical harmonic expansions of anomalous density, constitute relatively 'redder' sources: they contribute strength to the potential spectrum only in the degrees represented in the density distribution.

There are certainly a number of types of internal density heterogeneities that are appropriately modelled by discrete elements. Plum-pudding models of chemical heterogeneity (Davies 1984; Lay 1989) may be considered reasonably discrete, as can subducting slabs and hotspots swells. Even the density variations arising from the temperature structure of mantle convection have discrete characteristics such as horizontal boundary layers, rising and descending sheets and plumes, and isothermal cores. Thus there is ample justification for the use of discrete sources as modelling elements.

The observed potential spectrum for the Earth is characteristically reddened, with spectral strength decreasing as harmonic degree increases (e.g., Lerch *et al.* 1985a,b). If mantle heterogeneity can be reasonably represented by discrete sources, we will show in this paper that the redness of the observed potential spectrum requires an increase in the magnitude of these sources with depth.

2 STATISTICAL DISTRIBUTIONS OF INTERNAL MASS HETEROGENEITIES

2.1 Model distributions

There are many degrees of freedom in forward models for anomalous mass; for example, one might consider discrete sources of fixed magnitude, and investigate the dependence of the potential spectrum on their radial distribution; alternatively, the radial distribution of source locations could be held constant while varying the source strength as a function of depth. The most realistic approach would perhaps be to allow both of these functions to vary; however this would clearly give rise to an inexhaustible number of models to consider. If the viscosity of the mantle varies strongly with depth, as suggested for example by Davies (1984), Hager (1984), and Ricard, Vigny & Froidevaux (1989), then the capacity for supporting differential stresses associated with anomalous mass will also increase with depth. For this reason we will begin by following the second approach described above, with a fixed radial distribution of anomalous mass locations, and allow magnitudes to vary with depth. The present discussion will be restricted to mass anomalies within the mantle; later we will consider the effects of surface and core–mantle boundary topography.

In all of the following models, we begin by locating anomalous masses randomly throughout the volume of the mantle, i.e., with the following probability density functions:

$$f(r) \propto r^2, \qquad f(\phi) \propto \sin(\phi), \qquad f(\theta) = \text{constant}, \tag{1}$$

and then compute model potential spectra for different mass–depth functions. Generation of random variables with these prescribed probability functions is accomplished by means of a standard random number generating algorithm with a uniform probability density, and the following transformations:

$$\begin{aligned} r_i &= R[(R_c/R)^3(1 - x_{1i}) + x_{1i}]^{1/3}, \\ \phi &= \cos^{-1}[2(x_{2i} - 0.5)], \qquad \theta = 2\pi x_{3i}, \end{aligned} \tag{2}$$

where x_1, x_2, and x_3 are random numbers between 0 and 1, and i assumes values from 1 to k, where k is the total number of anomalous sources. This procedure produces a set of random locations for anomalous point masses, with a volumetrically uniform probability density throughout the mantle (Fig. 1).

Extension of these point masses into two or three dimensions (spherical caps or cones) in general results in a change in their centre of mass. For a spherical cap, the centre of mass is always located below the cap, i.e., $r'_{\text{centre}} < r'_{\text{cap}}$. For a spherical cone, the centre of mass may

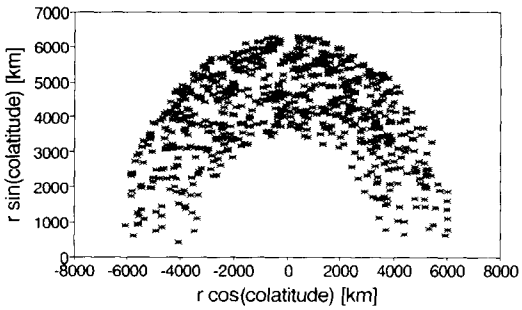

Figure 1. Distribution of radial location (r') and colatitude (ϕ) for a set of randomly located anomalous sources with volumetrically uniform probability density, generated by (1). The plot represents a meridional section onto which all locations have been projected by rotation about the axis of the spherical coordinate system.

lie above or below $\langle r \rangle$ (the mean of r_1 and r_2) depending upon the height and width of the cone. In order to enable a direct comparison of point mass and 2- or 3-D source models, we adjust the radial coordinates of spherical caps and cones to produce the same centres of mass as those in the corresponding point source model. The adjusted radial coordinates are

$$r_{i,\mathrm{cap}} = 2r_{i,\mathrm{point}}(\cos\alpha - 1)/(\cos^2\alpha - 1),$$
$$r_{i,\mathrm{cone}} = (4/3)r_{i,\mathrm{cap}}(r_2^3 - r_1^3)/(r_2^4 - r_1^4) \qquad (3)$$

(for an approximately equant cone, with $r_2 - r_1 = 2\alpha\langle r \rangle$).

Having generated randomly distributed source models in this way, we can assign masses to each anomalous source according to various mass–depth relationships. We will focus on one particular family of mass–depth laws:

$$M_i = x_{4i}[M_0 + M_1](d_i/d_{\mathrm{CMB}})^p] \qquad (4)$$

where x_4 is random ($-1 \le x_4 \le 1$), M_0 and M_1 are constant scale factors, and the exponent p is an experimental variable in the forward modelling.

In order to restrict our attention to plausible source models, several additional constraints must be applied. Because models of the Earth's potential assume the origin at the centre of mass, the first moments of the mass distribution should be vanishingly small [$\Phi(1) \approx 0$]. Additionally, we require the sum of the positive and negative anomalous masses to equal zero. The procedures described above for generating anomalous mass distributions generally satisfy these criteria when the number of anomalous masses is sufficiently large (of the order 10^3); for smaller numbers of discrete sources, random variations are relatively important, and several adjustments were necessary to approximately satisfy these conditions. First, in order to obtain a zero first moment, the geographic coordinates (θ, ϕ) and mass of the kth (last) source were adjusted to exactly cancel the vector sum of the other $k-1$ sources:

$$M_k X_k = -r_k \Sigma\,(M_i r_i \cos\theta_i \sin\phi_i),$$
$$M_k y_k = -r_k \Sigma\,(M_i r_i \sin\theta_i \sin\phi_i), \qquad (5)$$
$$M_k z_k = -r_k \Sigma\,(M_i r_i \cos\phi_i),$$

where x, y, and z are the adjusted Cartesian coordinates of the kth source, and the summation interval ranges from 1 to $k-1$. The second adjustment, to obtain zero-net anomalous mass, was accomplished by dividing the mantle into 10 depth intervals, calculating the scalar mean of the anomalous masses in each interval, and subtracting that mean from each anomalous source in the interval. This approximately preserved both the statistical properties of the initial mass–depth function (4) and the zero first moment.

Figure 2 illustrates the mass–depth characteristics of source models generated by the procedures above, with 100

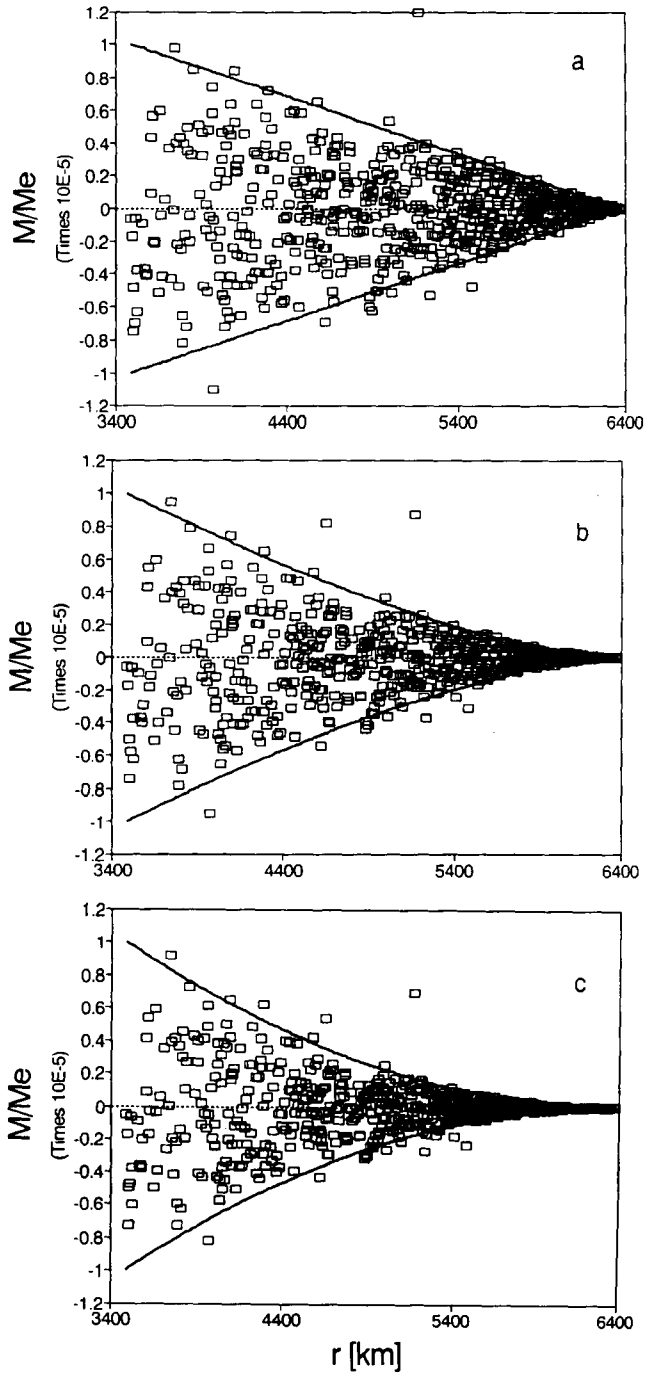

Figure 2. Mass–depth models with bounding values $M/M_{\mathrm{E}} = \pm 10^{-5}$ $(d/d_{\mathrm{CMB}})^p$; (a) $p = 1$; (b) $p = 1.5$; (c) $p = 2$. Corresponding potential spectra are illustrated in Fig. 3.

point mass anomalies in the same random locations for each model, but having different relative strengths as a function of depth. The mass–depth relation (4), with $M_0 = 0$, $M_1 = 10^{-5} M_E$, and $p = 1$, 1.5, or 2 (Figs 2a, b and c respectively) defines a set of envelopes which generally confines the individual sources. However, as a consequence of the adjustments for zero first moment and zero total anomalous mass, several of the anomalous source lie outside of these envelopes. In order to evaluate the effects of such deviations, as well as the effects of different random geographic source distributions, models were run in sets of 10, with identical mass–depth parameters but different random geographic and radial coordinates. When the spectra were computed and plotted, we found that in general about seven of the 10 spectra were similar in general trend (although different in detail as a consequence of variability in source locations), and that the models producing deviant spectra invariably had one or more source points lying far outside the mass–depth envelopes of (4) and Fig. 2, due to particular details of the random source locations. Such ill-behaved models were discarded.

2.2 Model spectra

We first consider point source models with $M_0 = 0$ and $p > 0$, that is, with mass anomalies that increase in magnitude with depth from a value of zero at the surface. Fig. 3 shows the potential spectra calculated for sets of models with $k = 100$ point masses and different values of p, corresponding to the envelope curves of Fig. 2. The individual model spectra are characterized by local maxima and minima superimposed on a smooth decay of strength with increasing harmonic degree. For each set of model spectra (Figs 3a, b and c; $p = 1$, 1.5, and 2 respectively), the general degree-dependent decay of $\Phi(n)$ is consistent within the set, whereas the local variability is unique for each model in the set. Examination of the spectra for individual models with identical source locations but different values of p [compare for example the uppermost curves in Figs 3(a), (b) and (c)] shows strong similarities in the local peaks and troughs, but fundamental differences in the general degree dependence of Φ. It clearly follows that the general degree dependence of Φ is determined by the common mass–depth relationship for each set of model spectra, whereas the local variability reflects the particular geography of the source distributions of the individual models.

Because the potential coefficients for monopole sources in equations (5), (6), (7), and (9) of paper I depend linearly upon (M_i/M_E), the spectra can be rescaled by multiplying each source mass by a constant factor; on a logarithmic plot such as Fig. 3, this corresponds to translating the spectrum upward or downward without changing its shape. Therefore in Fig. 3 and the figures to follow (unless otherwise noted), the spectra have been rescaled so that the mean log value of the set of model spectra at $n = 2$ is equal to the actual value of $\Phi(2)$ determined for the Earth. For models with M_1 of the order of $10^{-5} M_E$, the difference between the original and rescaled spectra is always relatively small (less than a factor of two), but because it facilitates comparison of shapes, we show the rescaled spectra, together with the observed spectrum of the Earth's gravitational field

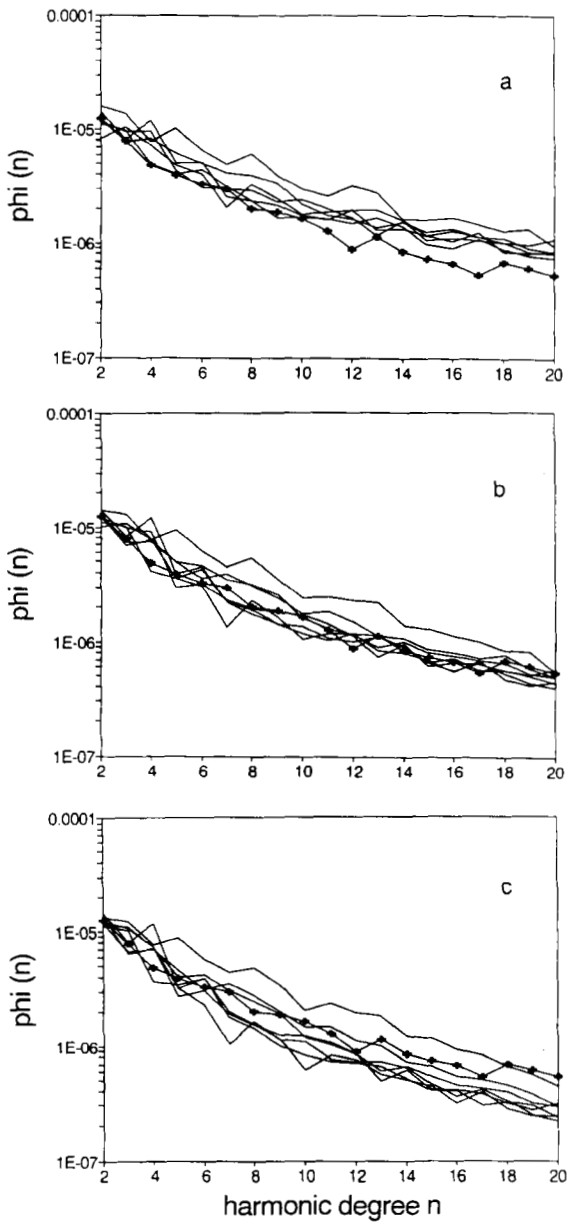

Figure 3. Potential spectra calculated for model sets of 100 point masses, scaled with depth as in Fig. 2. (a) $p = 1$; (b) $p = 1.5$; and (c) $p = 2$. GEM-L2 spectrum is shown with solid symbols for comparison; $p = 1.5$ yields the best match between models and GEM-L2.

represented by the GEM-L2 Earth model (Lerch *et al.* 1985a,b). In the degree range we consider (2–20), GEM-L2 is typical of most recent gravity models. This rescaling will enable us to determine an optimum value for the exponent p in (4), a parameter which affects only the shape of the spectrum. We will then return to the question of the actual magnitudes of the mass anomalies, and discuss the implications of the best model value of the mass scale factor below.

It is immediately apparent that the model spectra of Fig. 3(a) have too much relative strength in the higher harmonics in comparison with the GEM-L2 spectrum, indicating excessive shallow sources of anomalous mass. Higher values

of the exponent p result in smaller relative magnitudes for the shallow sources; for masses increasing as the square of depth ($p = 2$; Figs 2c, 3c), the model spectra are too red, i.e., too strongly diminished at high harmonic degrees. Fig. 3(b) shows that anomalous masses increasing according to $d^{1.5}$ generate model spectra that closely duplicate the curvature of the observed GEM-L2 geopotential spectrum.

The magnitude of the deep anomalies in Fig. 2 is quite large, but not unreasonably so. The rescaling described above ['pinning' the model spectra to $\Phi(2)$ of GEM-L2] decreases these source strengths by about 20 per cent, a negligible amount in the present discussion. The scale factor $M_1 = 10^{-5} M_E$ represents the upper limit of individual source strengths; if a mass anomaly of this magnitude were to be produced by CMB topography with a lateral dimension of 1000 km, it would require on the order of 10 km of relief. The mean (absolute value) of the anomalous masses near the CMB in these models is half of this scale value, with a proportional reduction of required topography. Thus anomalies of this size are compatible with seismologically derived estimates of CMB topography (e.g., Creager & Jordan 1986; Morelli & Dziewonski 1987). However, we will return to the question of CMB topography in a later discussion.

Next we consider non-zero mass anomalies at the surface ($M_0 > 0$). As shown in paper I, a surface point mass anomaly generates a flat or degree-independent potential spectrum. Although any geographic distribution of sources at the surface can give rise to a structured spectrum, with maxima and minima at particular values of n, the overall trend is still essentially flat. Therefore an upper bound on the plausible magnitudes of anomalous masses at the surface is imposed by the minimum value of $\Phi(n)$ over the degree range up to about $n = 20$, approximately 3 or $4 \times 10^{-7} M_E$. Here we will assume a value of $2.5 \times 10^{-7} M_E$ and investigate the characteristics of the internal mass–depth relationship that incorporates non-zero surface anomalies while still generating acceptable potential spectra. In a later section we will return to a discussion of mass anomalies at the surface, in the context of dynamic topography.

Figure 4(a) summarizes a set of source models with $M_0 = 2.5 \times 10^{-7} M_E$, $M_1 = 10^{-5} M_E$, and $p = 2$. The corresponding potential spectra are illustrated in Fig. 4(b), which shows that a good match to the observed spectrum is obtained with $p = 2$, in contrast to the case for $M_0 = 0$, where $p = 1.5$ yielded the best fit. Introducing non-zero mass anomalies at the surface thus requires even greater relative increases in source strength with depth, in order to generate spectra with the characteristics degree-dependence of the actual potential spectrum of the Earth.

If the anomalous sources are confined to the upper mantle [by replacing R_c with $R - 670$ in (2) and d_{CMB} with 670 km in (4)], no value of the exponent p is large enough to match the observed spectrum. Figs 5 and 6 respectively show upper mantle source models and corresponding potential spectra, with (a) $p = 3$, (b) $p = 5$, and (c) sources confined to 670 km depth in order to approximate an infinitely large p. All of the spectra have too much relative high-degree strength. Even in the limit of infinite p the spectrum remains too white. It seems clear that large mass anomalies are required in the lower mantle in order to produce the observed degree-dependence of the geopotential spectrum.

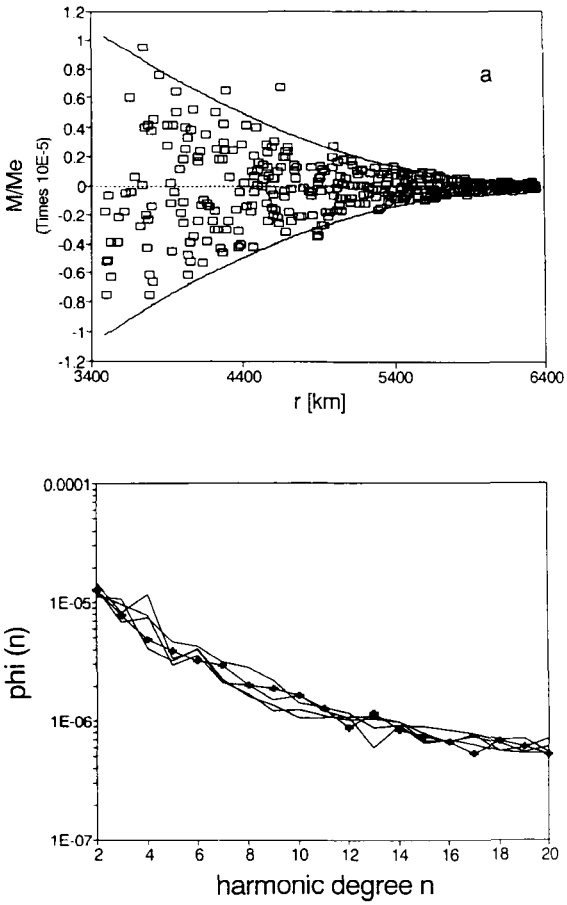

Figure 4. (a) Mass–depth models with bounding values $M/M_E = \pm[2.5 \times 10^{-7} + 10^{-5} (d/d_{CMB})^p]$; $p = 2$. These differ from the models of Fig. 2(c) by allowing non-zero anomalous magnitudes at the surface. (b) Corresponding potential spectra. GEM-L2 spectrum is shown for comparison; $p = 2$ yields an acceptable match.

The effects of finite-dimensional sources can be explored by replacing point masses with 2- and 3-D sources. Some model results are illustrated in Fig. 7, which shows the potential spectra for three sets of source models, each with exactly corresponding random source magnitudes and locations of centres of mass, but with different source dimensions. The differences in the potential spectra are generally most pronounced for $n \geq 10$. For 5° spherical cap sources, the concave-downward spectrum characteristic of a single cap (see Fig. 5 of paper I) gives rise to a high-degree spectral attenuation via the factor $(2n + 1)^{-2}$ in equation (6) of paper I. For n in the interval 2 to 5, however, there is little difference between the spectrum of a point mass and that of a spherical cap at the same depth; Fig. 7 shows that the same is also true for source ensembles. For sources expanded into spherical cones of roughly equant shape, the centre of anomalous mass is at a radius very close to $(r_1 + r_2)/2$ (within a fraction of a per cent). Nearly half of the anomalous mass of each source is therefore shallower than the corresponding point mass source, leading to a slight whitening of the spectrum. In general the differences between the spectra produced by point masses and distributed sources are much smaller than those associated

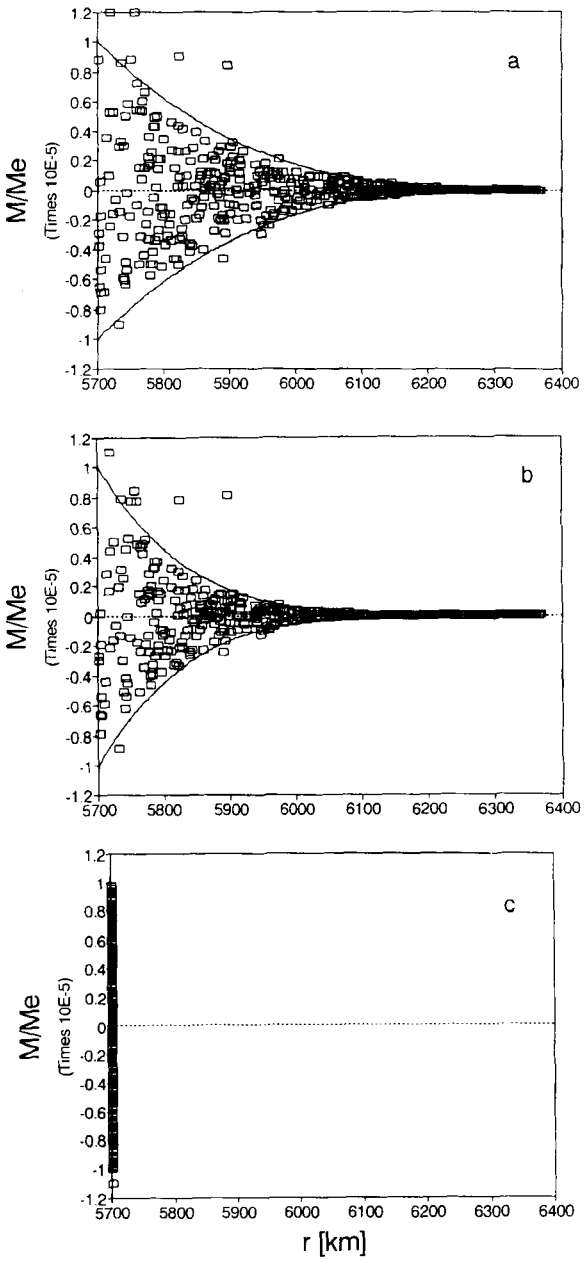

Figure 5. Upper mantle mass–depth models with bounding values $M/M_E = \pm 10^{-5}\ (d/670)^p$; (a) $p = 3$; (b) $p = 5$; (c) masses at $d = 670$ km only. Corresponding potential spectra are illustrated in Fig. 6. Note that the horizontal scale is different than in preceding figures.

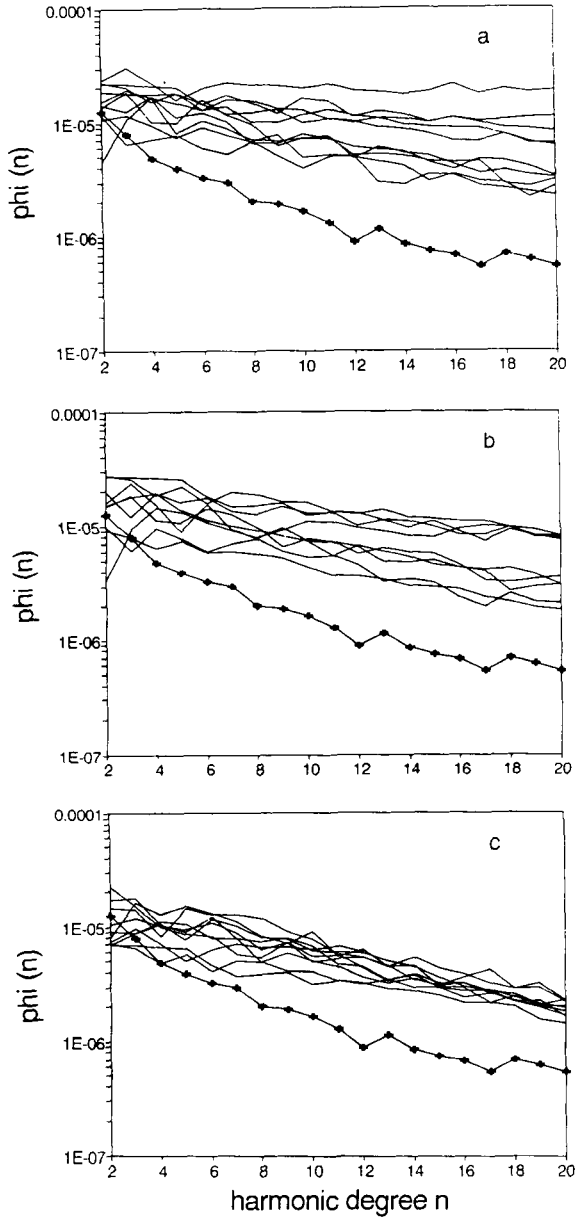

Figure 6. Potential spectra calculated for model sets of 100 point masses, restricted to the upper mantle and scaled with depth as in Fig. 5. GEM-L2 spectrum is shown for comparison; models with sources confined to 670 km depth yield a slightly better match than models with shallower sources, but still generate too much relative high-degree strength.

with different mass–depth laws; therefore we conclude that the dimensions of anomalous masses in the Earth are less important in shaping the geopotential spectrum than the distribution of mass with depth, at least over the degree range below about 10.

3 MASS ANOMALIES DUE TO DYNAMIC TOPOGRAPHY

3.1 Introduction

In the models of the preceding section, anomalous masses were assumed to be randomly distributed, with volumetrically uniform probability, throughout the entire mantle or confined to the upper mantle. These models are very general and conceptually process-independent. Additional constraints can be placed on the distribution of anomalous mass in the context of a dynamic Earth, in which negative mass anomalies rise buoyantly through the mantle, and positive mass anomalies sink. This vertical motion induces dynamic deformation of internal density discontinuities, with rising and sinking flows causing upward and downward deflections of the density interfaces, respectively (Hager 1984; Richards & Hager 1984; Hager *et al.* 1985). Depression of a horizontal density interface, due to the

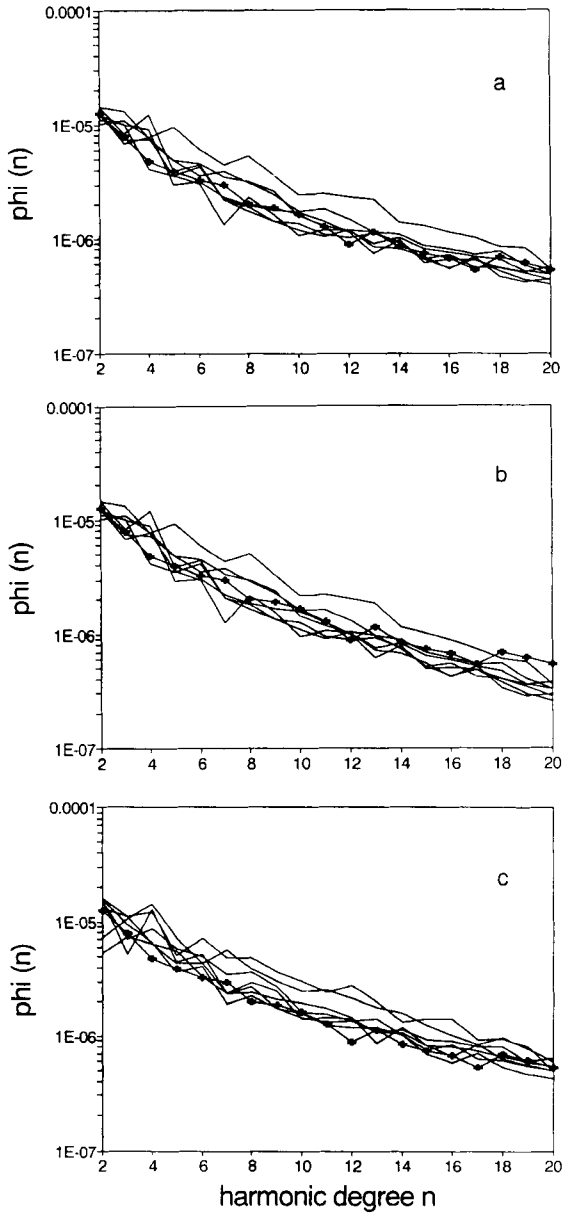

Figure 7. Potential spectra calculated for model sets of 100 discrete mass anomalies, scaled with depth as in Fig. 2 with $p = 1.5$. (a) Point masses; (b) spherical caps with 5° generating angle (10° diameter); and (c) approximately equant spherical cones with 5° generating angle. Source locations (centres of mass) are the same for corresponding models with each source geometry. GEM-L2 spectrum is shown for comparison. Caps generate slightly 'redder' spectra; cones slightly 'whiter'.

viscous flow driven by a dense sinking body, results in a negative mass anomaly where the interface is distorted. This has two consequences for our source models: first, although certain types of mass anomalies such as chemical heterogeneities may be approximately randomly located throughout the volume of the mantle, the distribution of anomalous masses will show concentrations at the depths of internal density discontinuities; and secondly, there will be a tendency for anomalies of opposite sign to occur in vertical alignment. In this section we examine the effects of these distribution characteristics on model potential spectra.

3.2 Topographic mass anomaly model

A rigorous analytical treatment of the dynamic deflection of density interfaces by isolated bodies in an otherwise uniform sphere is a problem beyond the scope of this paper; however we may draw upon the analysis of Koch & Ribe (1989) to guide us in formulating a simplified approximation. In particular, their analysis showed that a viscous spherical body of anomalous density, in the vicinity of a density interface in a viscous fluid halfspace, produces an axisymmetric anomalous topography on the interface, with an amplitude that varies directly with the density and viscosity contrasts, and inversely with the vertical distance separating the anomaly and the interface. The amplitude decay as a function of distance from the axis of symmetry is governed by the viscosity contrast in such a way that the *total* anomalous mass due to the topography (1) is largely independent of the viscosity contrast—the topography is broader and flatter for low contrasts, but represents the same anomalous mass as that accompanying high viscosity ratios; and (2) is equal in magnitude but of opposite sign to the anomalous mass, i.e., dynamically compensated, when the sphere is close to the interface.

The anomalous mass due to dynamic topography in such a model may be expected to diminish as the separation between the spherical anomaly and the density interface increases. Koch & Ribe (1989) show that the surface topography produced by a spherical anomaly at a depth greater than about 2 or 3 sphere radii is independent of the viscosity contrast; however the absolute dependence of topography on depth is not shown. Richards & Hager (1984) derive Green's functions relating surface potential at each spectral degree to the strength of internal 'driving' sources as a function of r'; these are identically zero at the upper and lower boundaries of the mantle, where the driving sources are perfectly compensated, and reach maximum values at different depths in the mantle for different harmonics and viscosity structures. This spectral decomposition is not readily applied to discrete sources; therefore we model the dependence of a topographic mass anomaly on the proximity and magnitude of the driving internal mass anomaly by a simple power law:

$$M_{i,\mathrm{topo}} = -M_i(dz/z_0)^Q \qquad (6)$$

where $M_{i,\mathrm{topo}}$ is the mass anomaly due to the topography produced on a density boundary due to the flow driven by a mass anomaly M_i at a vertical distance dz from the boundary, and z_0 is a scale factor approximately equal to the radius of the mass anomaly; we will use a value of 100 km for z_0. The exponent Q (≤ 0) is related in a general way to the viscosity, or to the vertical flow velocity gradients associated with the internal anomalies: the value $Q = 0$ means that the (integrated) boundary deflection is independent of distance from a sinking or rising heterogeneity, while large negative values of Q indicate that internal anomalies have a negligible effect on the flow field at a distance larger than the scalelength of the anomaly. We wish to investigate the effects on the potential spectrum of varying the value of the exponent Q.

Because the density contrasts across the free surface and across the core–mantle boundary are nearly an order of magnitude larger than that of any other discontinuity in the

Earth, we will restrict the dynamic anomalous masses in our models to those two interfaces. Each of the internal mass anomalies of our model ensemble produces two additional anomalies of opposite sign with the same geographic coordinates, one at the CMB and one at the surface, with magnitudes governed by (25). We will hold the parameters of the mass–depth relation (4) fixed at $M_0 = 2.5 \times 10^{-7} M_E$, $M_1 = 10^{-5} M_E$, and $p = 2$, and consider Q between -1 and -4.

3.3 Potential spectra for dynamic mass models

Figures 8 and 9 illustrate source models and corresponding potential spectra for different values of Q. For large

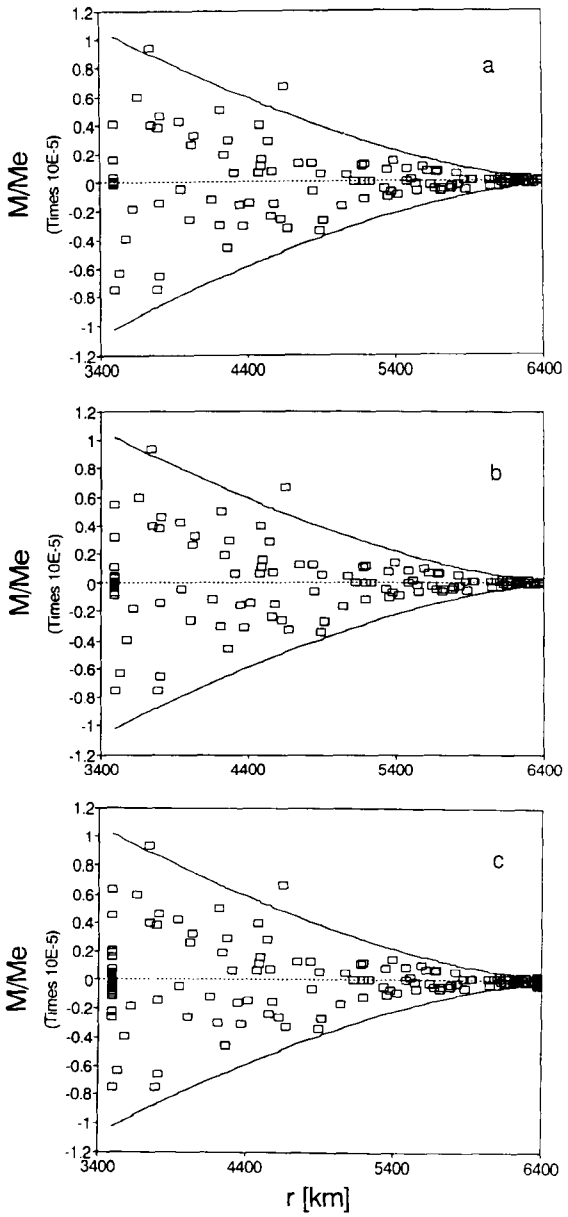

Figure 8. Mass–depth models with bounding values for internal 'driving' sources $M/M_E = \pm[2.5 \times 10^{-7} + 10^{-5}\ (d/d_{CMB})^2]$; to simulate dynamic topography each driving anomaly produces a topographic mass anomaly of opposite sign at the surface and on the CMB, with magnitude proportional to that of the driving source and decreasing with source–interface separation dz according to $M_{i,\text{topo}}\ dz^Q$. (a) $Q = -4$; (b) $Q = -2$; (c) $Q = 1$. Corresponding potential spectra are illustrated in Fig. 9.

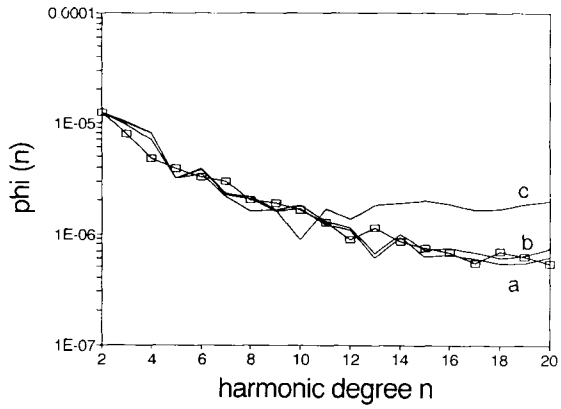

Figure 9. Potential spectra calculated for model sets of 100 point masses, with corresponding dynamic mass anomalies as in Fig. 8. (a) $Q = -4$; (b) $Q = -2$; (c) $Q = -1$. GEM-L2 spectrum is shown for comparison; $Q = -1$ generates too much relative high-degree spectral strength, due to excessive surface topographic mass anomalies.

negative values of Q, the topographic mass anomalies are all small compared to the internal anomalies, and the potential spectrum is indistinguishable from one with no topographic anomalies (compare Figs 4b and 9). When the magnitude of a topographic mass anomaly decays linearly with distance to the internal anomalous source (i.e., $Q = 1$), some of the surface anomalies produced by mid- or deep mantle heterogeneities become larger than M_1, the limiting magnitude for anomalies in the upper few hundred kilometres of the mantle (Fig. 8), resulting in excessive high-degree spectral strength (Fig. 9). Strong or moderate coupling ($Q \geq -1$) of surface topography to large deep mass anomalies thus results in a radial distribution of anomalous mass that is incompatible with the constraint imposed by the observed geopotential spectrum.

As discussed above, an absolute upper bound on the anomalous mass associated with non-isostatic long-wavelength (up to $\alpha \approx 20°$) surface topography (or any other non-isostatic shallow mass anomalies), approximately 3 to $4 \times 10^{-7} M_E$, is imposed by the minimum value of $\Phi(n)$ over the internal up to about $n = 20$. Compensated mass anomalies may be larger by a factor of r'/h (the inverse of the dipole factor discussed in paper I), where h is related to the depth of compensation; this factor is of the order of 100 for isostatic compensation, but only two or three for dynamic compensation by lower mantle sources. This gives an absolute upper bound of approximately $10^{-6} M_E$ for surface mass anomalies maintained dynamically by deep mantle driving sources. A tighter but still approximate upper bound of roughly $3 \times 10^{-7} M_E$ is suggested by Figs 8 and 9. The Phanerozoic history of marine transgressions onto the continents places an upper limit on the amplitude of dynamically maintained surface topography of approximately 100 to 150 m (Gurnis 1990a,b). For an areally weighted average density contrast between the lithosphere, hydrosphere and atmosphere of approximately 2300 kg m^{-3}, and a diameter of 3000 km, this dynamic topography corresponds to mass anomalies in the neighbourhood of $2.5 \times 10^{-7} M_E$. Thus our estimate based on Figs 8 and 9 appears reasonable.

Because of the possibility that viscosity increases

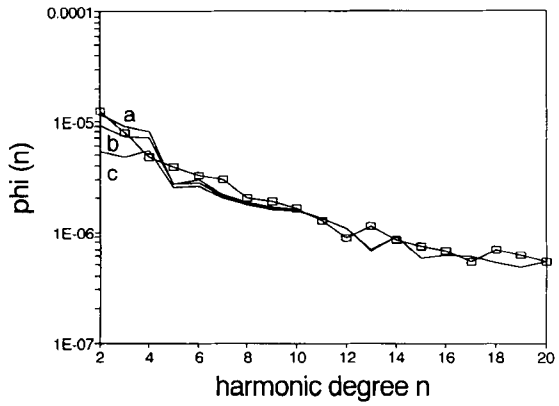

Figure 10. Potential spectra calculated for model sets of 100 point masses with corresponding dynamic mass anomalies as in Fig. 8, but only on the CMB. (a) $Q = -1$; (b) $Q = -0.5$; (c) $Q = -0.05$. GEM-L2 spectrum is shown for comparison; as Q approaches zero, the sources become radial dipoles and lose low-degree spectral strength.

significantly with depth in the mantle, the production of dynamic mass anomalies at the upper and lower boundaries may not be symmetric, as it is in our model above; larger mass anomalies would be expected at the lower interface (e.g., Hager 1984). As a limiting case, we have examined a set of models with dynamic deflection of only the lower boundary of the mantle. As shown in Fig. 10, there is little effect on the potential spectrum, unless the CMB topography is strongly linked to flow driven by internal mass anomalies ($-1 < Q \leq 0$). For $Q = 0$, every internal heterogeneity produces an equal anomaly of opposite sign on the CMB, and the source ensemble takes on the characteristics of an ensemble of dipoles. This is reflected in the model potential spectra (Fig. 10), where the relative low-degree strength is reduced, as shown in paper I for individual dipole sources (Fig. 6 of paper I). Note that in Fig. 10 the spectra have not been rescaled to match the GEM-L2 value of $\Phi(2)$.

This result has an important implication for the relationship between the low-degree harmonics of the geopotential and CMB topography. Because neither the core nor mantle is rigid, it is obvious that distortion of that interface must be either isostatically compensated (e.g., by anomalously dense material at the base of the mantle), or dynamically maintained by mantle flow. In either case, a negative topographic mass anomaly on the CMB must be overlain by a positive internal anomaly of comparable magnitude; together these comprise an essentially dipolar source, which may not contribute significantly to the low-degree potential at the surface.

Several types of relatively high-density heterogeneities may occur within or at the base of the mantle, such as subducted slabs (Silver & Carlson 1988), refractory residue from core differentiation (Ruff & Anderson 1980), or primitive mantle material (Silver & Carlson 1988). Because of the extreme density contrast across the CMB, these heterogeneities will collect there, resting upon the core. Such a heterogeneity, with a local thickness of 200 km and a density anomaly of 3 per cent, would be sufficient to generate about 6 km of isostatically compensated core topography. The surface potential due to such a mass dipole is much less than would be generated by the topography alone; the factor h/r' (paper I) reduces the dipole contribution to about 3 per cent of that of the monopole. We have shown above that monopole sources approaching $10^{-5} M_E$ in the lower mantle can produce the observed low-degree spectrum at the surface; to achieve the same low-degree strength, dipole sources must be roughly 30 times larger. Thus isostatic topography at the CMB, while it may be considerable in magnitude, will not necessarily produce significant geoid effects at the surface.

Dynamically maintained topography also constitutes an essentially dipolar source, but it may differ significantly from isostatic topography in two important ways. First, the pole separation h may be significantly increased, and the dipole 'reduction factor' h/r' concomitantly less extreme. Further, as h increases, dynamic compensation is less completely maintained: the mass anomaly due to topography becomes smaller than the driving anomaly, which thus becomes more monopolar and contributes more to the surface potential. This effect was considered by Hager (1984) and Richards & Hager (1984), and can be seen in their 'dynamic response' functions. It is important to note that the principal contribution to the measured potential comes not from the CMB topography, but from the internal partially compensated mantle heterogeneity; dynamically generated CMB topography serves to diminish geoid anomalies, by partial compensation, rather than to generate them. This leads to two conclusions: (1) the geopotential spectrum only weakly constrains the magnitude of CMB topography, if at all; even high amplitude compensated topography will produce only minor effects on the geoid; and (2) generation of the observed low-degree characteristics of the geopotential spectrum requires at least some of the large, deep internal anomalies to be essentially monopolar, in other words, not too strongly coupled dynamically to CMB topography. Decoupling could perhaps be accomplished by a low-viscosity thermal boundary layer at the base of the mantle (e.g., Stacey & Loper 1983); however, our models clearly do not require such a layer. In fact we can rule out only the strongest coupling ($-1/Q \gg 1$), or nearly complete dynamic compensation.

4 DISCUSSION OF MODELLING RESULTS

Although the locations and characteristics of the internal mass anomalies that generate the Earth's non-hydrostatic gravitational potential can never be uniquely determined from measurements of the field at the surface, the spectral characteristics of the geopotential do provide general information on the statistical distribution of internal density heterogeneities. The contribution to the spectrum at the surface by sources at depth is attenuated in a degree-dependent manner; because of this the upward convexity of the observed spectrum can best be explained in terms of large deep sources, producing the low-degree strength, and smaller shallower sources generating the higher harmonics.

This is in general agreement with the conclusions drawn previously by Lowrey (1978), Cook (1980), and Bowin (1983, 1986). However it conflicts with that of Lambeck (1976), who suggested that the geopotential spectrum could be accounted for by density anomalies with a 'white noise' distribution in the uppermost 1000 km of the mantle, and

that deep mantle anomalies must be relatively small, corresponding to 200 m or less of uncompensated CMB topography. This disagreement may be attributable in part to a difference in analytical methods: a truncated harmonic expansion employing continuous functions of anomalous density inevitably produces smoother source models than discrete anomalous sources, and therefore generates less relative strength in the high degrees of the potential spectrum. Thus discrete source models, such as ours and the point mass models of Lowrey (1978), naturally require more substantial deep sources than are demanded by continuous source models. Perhaps more importantly, Lambeck's model does not fully account for the curvature of the spectrum, generating too little strength in the low ($n = 2$, 3) and high ($n \geq 15$) harmonics, and excessive strength in the intermediate range. It is precisely this curvature that requires increasing source strength with depth.

It is instructive to compare the geopotential spectrum with the geomagnetic spectrum (Merrill & McElhinny 1983). The source regions for the non-hydrostatic gravitational and magnetic fields are strongly complementary: due to the low viscosity of the core, lateral density gradients cannot be maintained, so that no sources of the anomalous geopotential can be expected within the core; conversely, mantle temperature exceed the Curie point of any natural magnetic material, and the viscosity and conductivity are clearly inappropriate to generate magnetic fields by dynamo action. Thus the geopotential spectrum arises entirely from sources in the mantle and crust, while the sources of the magnetic spectrum are confined to the core and the crust. The wide radial separation of the two magnetic source regions is clearly reflected in the degree-dependence of the geomagnetic spectrum, with two fairly linear segments corresponding unambiguously to the source regions: the steeply sloping segment from $n = 2$ to 8 is attributable to core sources; the shallow segment for $n \geq 12$ derives primarily from crustal magnetization (Merrill & McElhinny 1983).

In contrast, the gradual change in slope of the geopotential spectrum suggests, although it does not require, a continuous distribution of sources extending through the entire depth range of the mantle. Our modelling results indicate that the contribution to the potential spectrum of any particular depth interval of the mantle has an overall degree-dependence that is determined most strongly by depth; the geographic distribution or dimension of sources in each interval may produce particular spectral peaks or holes, but not the general decay of $\Phi(n)$ with increasing n. In order to generate a smoothly curved spectrum, there must be contributions from sources at a number of different depths, with source amplitudes generally increasing with depth.

This is a general conclusion that does not depend in any way upon assumed models of viscous flow or on the nature of the mass anomalies. While we have considered only continuously varying mass–depth laws (4) and quasi-continuous radial distributions of source locations (that is, the discrete sources are not confined to discrete ranges of r'), it is not difficult to conclude that more discontinuous models will still have to satisfy the same basic constraint of source strengths increasing with depth, extending into the deep mantle.

The conclusion that source magnitudes increase with depth in the mantle does not conflict with the association of particular harmonic intervals with specific source distributions, as proposed by many investigators. Clearly this idea accords with the high-degree harmonics being related to surface topography. The degree range 4 to 10 may be associated with slab penetration into the lower mantle and resultant depression of the CMB, as inferred by Hager (1984). However we would suggest that there must be additional deep sources as well. If a particular mass anomaly due to CMB topography is, as it must be, less than or equal to that of the driving source (for example, a slab), then the topographic contribution to the geopotential is smaller for all positive n than that of the slab, and the total spectral contribution of the system is less strongly degree-dependent than that of the Earth. This is in fact shown in Fig. 7 of Hager (1984). Additionally, as Hager notes, the slab model accounts for roughly 40 per cent of the variance in the spectrum for degrees 4–9, which is substantial, but which still leaves 60 per cent to be accounted for by other sources; we would suggest that these are dominantly in the deep mantle.

Thus we suggest that the dominant sources of the degree 2–4 geopotential are to be found in the lower mantle. If, as we argue, dynamic deflection of the CMB is not the principal source of the low-degree anomalous potential at the Earth's surface, these harmonics must be related to monopolar density anomalies associated with lateral temperature gradients or chemical heterogeneities in the deep mantle.

The magnitudes of these monopolar lower mantle mass anomalies must be substantial. Because of the general insensitivity of our model spectra to the dimensions of the anomalous sources, we are able to translate mass anomalies into density anomalies only by making assumptions about their volumes. Seismological evidence suggests lateral heterogeneities in the lower mantle with both short and long scalelengths (e.g., Haddon 1982; Snoke & Sacks 1986). Snoke & Sacks (1986) conclude that the dominant length-scale of lowermost mantle heterogeneity is 200 km, but that there is also variability with length-scales of 1000 km. For lower mantle sources with horizontal dimensions of the order of 1000 km and a vertical extent of 100 km, a mass anomaly of $10^{-5} M_E$ corresponds to a density anomaly of approximately 600 kg m^{-3}, or roughly a 10 per cent departure from the mantle density at the CMB. Clearly this estimate seems large and is highly uncertain, but if such density anomalies exist, they are unlikely to be entirely of thermal origin. Lateral temperature variations in the upper mantle may be as large as 100 °C (between the interiors of subducted slabs and regions below mid-ocean ridges); for a thermal expansion coefficient of the order of 10^{-5} K^{-1}, this corresponds to a density variation of about 1 per cent. In the lower mantle, the magnitude of lateral temperature variations is less well constrained, but is probably not widely different. Thus it appears, somewhat by default, that chemical heterogeneities in the deep mantle may be important sources of the degree 2–4 potential.

Various lines of geochemical and geophysical evidence suggest the existence of chemically distinct heterogeneities within the mantle. Davies (1984) summarizes some of the isotopic and geochemical evidence for the existence of

several distinct reservoirs within the mantle, as well as geophysical constraints. Detailed studies of seimsic travel-time residuals (e.g., Dziewonski 1984) and of the systematics of particular phases (e.g., Young 1990) suggest strong lateral heterogeneity, especially in the lowermost mantle. Lay (1989) and Young (1990) have suggested a 'plum-pudding' model of chemical heterogeneity within the mantle, similar to that of Davies (1984), in order to explain both the existence and lateral discontinuity of a heterogeneous layer at the base of the mantle. The density contrasts associated with chemical heterogeneity may be quite variable, and could plausibly exceed those associated with temperature. Material with excessively large density anomalies will tend to collect at the top or the base of the mantle as a consequence of buoyant forces, and will generally tend to be compensated. However, heterogeneities at some distance above the CMB may be sufficiently uncompensated to generate the low harmonics of the potential at the Earth's surface.

6 CONCLUSIONS

Our modelling results enable us to draw several specific inferences regarding the radial distribution of anomalous mass in the mantle. First, it is clear that the depth distribution of anomalous mass is more important in controlling the general degree-dependence of the geopotential spectrum than either the dimensions of the anomalous sources or their geographic (latitude/longitude) distribution. The geography of the source distribution produces 'structure' in the spectrum, i.e., local maxima and minima at particular harmonics, but exerts little or no control on the smoothed degree-dependence. Source dimension, i.e., the scale of heterogeneity, does affect the general shape of the spectrum; however models with discrete anomalous sources of reasonable (less than continental) length scale, confined to the upper mantle, are incapable of producing potential spectra with the same degree dependence as that of the real Earth. One must therefore conclude that the sources of the low harmonics are located principally in the lower mantle. The general decay of the spectrum of the Earth can best be explained in terms of sources at a number of different depths, with source amplitudes generally increasing with depth.

An additional major conclusion of this study is that the geopotential spectrum places only weak constraints on the amplitude of core–mantle boundary topography. Isostatically and/or dynamically compensated topography represents an essentially dipolar source ensemble, which may not contribute significantly to the low-degree harmonics ($2 \leq n \leq 4$) at the surface. Dynamically generated CMB topography serves to diminish geoid anomalies, by partial compensation of mobile mantle heterogeneities, rather than to generate them. The lower mantle mass anomalies that generate the low-degree spectral strength at the surface must be largely monopolar, and are therefore probably not directly associated with CMB topography.

ACKNOWLEDGMENTS

Stephen Sutton was supported by a National Science Foundation Graduate Fellowship.

REFERENCES

Bowin, C., 1983. Depth of principal mass anomalies contributing to the earth's geoidal undulations and gravity anomalies, *Mar. Geod.*, **7**, 61–100.

Bowin, C., 1986. Topography at the core–mantle boundary, *Geophys. Res. Lett.*, **13**, 1513–1516.

Bowin, C., Scheer, E. & Smith, W., 1986. Depth estimates from ratios of gravity, geoid, and gravity gradient anomalies, *Geophysics*, **51**, 123–136.

Cook, A. H., 1980. *Interiors of the Planets*, Cambridge University Press, New York.

Creager, K. C. & Jordan, T. H., 1986. Aspherical structure of the core–mantle boundary from PKP travel times, *Geophys. Res. Lett.*, **13**, 1497–1500.

Davies, G. F., 1984. Geophysical and isotopic constraints on mantle convection: an interim synthesis, *J. geophys. Res.*, **89**, 6017–6040.

Dziewonski, A. M., 1984. Mapping the lower mantle: determination of lateral heterogeneity in P-velocity up to degree and order 6, *J. geophys. Res.*, **89**, 5929–5952.

Gurnis, M., 1990a. Bounds on global dynamic topography from Phanerozoic flooding of continental platforms, *Nature*, **344**, 754–756.

Gurnis, M., 1990b. Plate-mantle coupling and continental flooding, *Geophys. Res. Lett.*, **17**, 623–626.

Haddon, R. A. W., 1982. Evidence for inhomogeneities near the core–mantle boundary, *Phil. Trans. R. Soc. Lond.*, A, **306**, 61–70.

Hager, B. H., 1984. Subducted slabs and the geoid: constraints on mantle rheology and flow, *J. geophys. Res.*, **89**, 6003–6015.

Hager, B. H., Clayton, R. W., Richards, M. A., Comer, R. P. & Dziewonski, A. M., 1985. Lower mantle heterogeneity, dynamic topography, and the geoid, *Nature*, **313**, 541–545.

Koch, D. M. & Ribe, N. M., 1989. The effect of lateral viscosity variations on surface observables, *Geophys. Res. Lett.*, **16**, 535–538.

Lambeck, K., 1976. Lateral density anomalies in the upper mantle, *J. geophys. Res.*, **81**, 6333–6340.

Lay, T., 1989. Structure of the core–mantle transition zone: a chemical and thermal boundary layer, *EOS, Trans. Am. geophys. Un.*, **70**, 49.

Lerch, F. J., Klosko, S. M., Patel, G. B. & Wagner, C. A., 1985a. A gravity model for crustal dynamics (GEM-L2), *J. geophys. Res.*, **90**, 9301–9311.

Lerch, F. J., Klosko, S. M., Wagner, C. A. & Patel, G. B., 1985b. On the accuracy of recent Goddard gravity models, *J. geophys. Res.*, **90**, 9312–9334.

Lowrey, B. E., 1978. Lateral density anomalies and the earth's gravitational field. *Rep. No. NASA TM-79554*, NASA-Goddard SFC, Greenbelt, MD.

Merrill, R. T. & McElhinny, M. W., 1983. *The Earth's Magnetic Field: Its History, Origin, and Planetary Perspective*, Academic Press, New York.

Morelli, A. & Dziewonski, A. M., 1987. Topography of the core–mantle boundary and lateral heterogeneity of the liquid core, *Nature*, **325**, 678–683.

Phillips, R. J. & Lambeck, K., 1980. Gravity fields of the terrestrial planets: long-wavelength anomalies and tectonics, *Rev. Geophys. Space Phys.*, **18**, 27–76.

Ricard, Y., Vigny, C. & Froidevaux, C., 1989. Mantle heterogeneities, geoid, and plate motion: a Monte Carlo inversion, *J. geophys. Res.*, **94**, 13 739–13 754.

Richards, M. A. & Hager, B. H., 1984. Geoid anomalies in a dynamic earth, *J. geophys. Res.*, **89**, 5987–6002.

Ruff, L. J. & Anderson, D. L., 1980. Core formation, evolution, and convection: a geophysical model, *Phys. Earth planet. Inter.*, **21**, 181–201.

Silver, P. G. & Carlson, R. W., 1988. Deep slabs, geochemical heterogeneity, and the large-scale structure of mantle convection, *Ann. Rev. Earth planet. Sci.*, **16,** 477–541.

Snoke, J. A. & Sacks, I. S., 1986. Seismic modelling of lateral heterogeneity at the base of the mantle, *Geophys. J. R. astr. Soc.*, **86,** 801–814.

Sutton, S. T., Pollack, H. N. & Jackson, M. J., 1991. Spherical harmonic representation of the gravitational potential of discrete spherical mass elements, *Geophys. J. Int.*, **107,** 77–82.

Stacey, F. D. & Loper, D., 1983. The thermal boundary layer interpretation of D″ and its role as a plume source, *Phys. Earth planet. Inter.*, **33,** 45–55.

Young, C. J., 1990. Excursions to the base of the mantle, *PhD dissertation,* University of Michigan, Ann Arbor.